JOURNAL OF GEOPHYSICAL RESEARCH: ATMOSPHERES, VOL. 118, 1–16, doi:10.1002/jgrd.50196, 2013

Microphysical simulations of large volcanic eruptions: Pinatubo and Toba

Jason M. English,[1] Owen B. Toon,[2] and Michael J. Mills[1]

Received 12 September 2012; revised 4 January 2013; accepted 17 January 2013.

[1] Simulations of stratospheric clouds from eruptions ranging in size from the 1991 eruption of Mount Pinatubo to that of Toba 74,000 years ago have been completed using a 3D microphysical sectional aerosol model advectively coupled to a general circulation model with prognostic chemistry (Whole Atmosphere Community Climate Model/ Community Aerosol and Radiation Model for Atmospheres). For Pinatubo, properties of the aerosol cloud peak within the ranges derived from observations in the Northern Hemisphere, but reduce faster than observed, and a general low bias is found in the Southern Hemisphere. These biases could be reduced by adding aerosol radiative coupling, a quasi-biennial oscillation, and the Cerro Hudson eruption to the model. Simulations of eruptions 10 times and 100 times larger than Pinatubo suggest burdens and Aerosol Optical Depth increase less than linearly (a 100-fold injection increase produces a 20-fold AOD increase) due to particle growth and sedimentation, consistent with previous work that also found the radiative forcings from large eruptions to be self-limiting. Global-averaged AOD remains elevated for 1, 2, and 4 years, respectively, for the three simulated eruptions. The inclusion of van der Waals forces in our coagulation scheme increases peak effective radius and reduces peak AOD by about 10–20%, with bigger effects for larger eruptions. Our simulations find peak mode size to vary by up to an order of magnitude and mode width to vary by up to 50%, suggesting that two-moment modal models may not accurately capture the evolving size distribution. These simulations suggest the value of including van der Waals forces in the coagulation scheme and sectional size distributions in climate models.

Citation: English, J. M., O. B. Toon and M. J. Mills (2013), Microphysical simulations of large volcanic eruptions: Pinatubo and Toba, *J. Geophys. Res. Atmos.*, *118*, doi:10.1002/jgrd.50196.

1. Introduction

[2] Volcanic eruptions can inject large quantities of SO_2 into the stratosphere, forming sulfate aerosols that perturb radiative forcing and stratospheric chemistry. Rare super-eruptions can potentially cause climate changes that are severe enough to trigger food shortages or biological extinctions [*Ambrose*, 1998]. Studying large eruptions can clarify the contributions of historical volcanic eruptions to past climate changes, the potential consequences of future volcanic eruptions on climate, and act as analogues for understanding hypothetical climate geoengineering schemes involving stratospheric sulfur injection [*Crutzen*, 2006].

[3] The size and width of the stratospheric aerosol size distribution, which affects the climate response, have been observed to significantly shift after volcanic eruptions [*Deshler*, 2008]. Representing this shift is important to accurately characterize the chemical, radiative, and dynamical responses in the stratosphere. Early microphysical simulations using 1D sectional models suggested that climate effects may be self-limiting in larger eruptions due to particle growth [*Pinto et al.*, 1989]. Similarly, simulations of hypothetical climate geoengineering stratospheric sulfur injection studies using sectional aerosol models predict stratospheric aerosol size distributions to shift in significant ways as injections increase in mass [*Heckendorn et al.*, 2009; *English et al.*, 2012]. For computational efficiency, modeling studies often parameterize microphysical process and/or the representation of size distributions. "Bulk aerosol" modules prescribe mode peak size and width of the aerosol size distribution [*Timmreck et al.*, 1999; *Oman et al.*, 2006; *Robock et al.*, 2009; *Aquila et al.*, 2012], while "modal aerosol" modules treat aerosol size in a series of size modes of prescribed lognormal shape and mode widths while allowing the peak size to evolve [*Niemeier et al.*, 2009; *Timmreck et al.*, 2010]. However, intercomparison studies have found that sectional models are more accurate than modal models when representing stratospheric aerosol size distributions after volcanic eruptions [*Weisenstein et al.*, 2007; *Kokkola et al.*, 2009]. Additionally, laboratory studies have found that the coagulation rate of sulfate aerosols increases due to the contribution of interparticle van der Waals

[1]NCAR Earth System Laboratory, National Center for Atmospheric Research, Boulder, CO, 80305, USA.
[2]Laboratory for Atmospheric and Space Physics, Department of Atmospheric and Oceanic Sciences, UCB 600, University of Colorado, Boulder, CO, 80303, USA.

Corresponding author: Jason M. English, NCAR Earth System Laboratory, National Center for Atmospheric Research, 1850 Table Mesa Drive, Boulder, CO 80305, USA. (jayenglish@gmail.com)

2169-897X/13/10.1002/jgrd.50196

forces [*Chan and Mozurkewich*, 2001]. Model simulations of ambient stratospheric aerosol have found the inclusion of these forces important to accurately represent the observed aerosol number concentration [*English et al*., 2011], yet van der Waals forces are not included in modeling studies of volcanic aerosols to date. In this paper, we utilize a sectional aerosol model that includes van der Waals forces in the coagulation scheme to study three eruptions in detail: the largest eruption of the past century (Mount Pinatubo in 1991), a hypothetical eruption ten times as large, and the largest eruption of the past 100,000 years (the Younger Toba Tuff, or "Toba" approximately 74,000 years ago).

[4] The 1991 eruption of Mt Pinatubo in the Philippines (15°N, 120°E) significantly perturbed stratospheric chemistry and aerosols, as observed by numerous instruments. The eruption injected 14–23 Tg of sulfur dioxide (SO_2) (7–11.5 Tg S) into the stratosphere [*Read et al*., 1993; *Krueger et al*., 1995; *Guo et al*., 2004], mostly on 15 June 1991. The SO_2 was converted to H_2SO_4 with an *e*-folding time of 35 days [*Bluth et al*., 1992; *Read et al*., 1993] or 23–25 days [*Guo et al*., 2004]. The eruption occurred during the easterly phase of the quasi-biennial oscillation (QBO), which caused the volcanic cloud to move westward and encircle the earth in about a month [*Baldwin et al*., 2001]. In the first months after the eruption, most of the aerosol burden was within the region between 20°S and 30°N [*McCormick and Veiga*, 1992; *Stowe et al*., 1992]. Stratospheric aerosol effective radius increased from about 0.2 μm to a peak of 0.6 μm nine months after the eruption and remained elevated for more than 2 years after the eruption [*Russell et al*., 1996]. A reduction in global net radiative flux of about 3 W m^{-2} was measured in summer and fall 1991 [*Minnis et al*., 1993]. The lower stratosphere warmed by 2–3 K [*Labitzke and McCormick*, 1992; *Labitzke*, 1994], and the lower troposphere cooled by about 0.5 K [*Dutton and Christy*, 1992]. By spring 1992, the stratospheric aerosol burden had reached its peak and began to subside [*Ansmann et al*., 1997]. Four to five years after the eruption, the background aerosol level was again present, but began to increase starting in 1998 through the present day due to several small eruptions [*Vernier et al*., 2011].

[5] Early simulations of the Pinatubo volcanic cloud using a GCM with chemistry and some aerosol microphysics found good agreement with SO_2 observations but not with aerosol observations, which the authors attributed to the lack of homogeneous nucleation in the model [*Bekki and Pyle*, 1994]. Early microphysical simulations found that including aerosol radiative heating increased transport of the aerosol cloud to higher latitudes and to the Southern Hemisphere, in better agreement with observations [*Young et al*., 1994]. Simulations using GCMs with sulfur chemistry and radiatively coupled bulk aerosols found good agreement with observed peaks in global optical depth but did not reproduce the persistence of observed tropical optical depth [*Timmreck et al*., 1999; *Oman et al*., 2006]. The authors attributed the discrepancy to overly vigorous transport from the tropical stratosphere to high latitudes due to the lack of QBO in their models, which is supported by observations [*Trepte and Hitchman*, 1992] and model simulations [*Graf et al*., 1993; *Stenchikov et al*., 2004; *Thomas et al*., 2009]. Recent simulations using a GCM with a bulk aerosol module with and without aerosol heating suggest that aerosol heating prolongs the radiative effect in the Northern Hemisphere, but the inclusion of QBO is needed for cross-hemispheric transport [*Aquila et al*., 2012]. Simulations using a GCM with a modal aerosol model suggested that inclusion of ash in the model did not significantly contribute to the evolution of the aerosol distribution [*Niemeier et al*., 2009]. However, observations of large dust particles in the Arctic months after the Pinatubo eruption suggest significant radiative heating due to the dust [*Pueschel et al*., 1994]. Another study using a GCM with a modal aerosol model found that changing the season of the eruption affected the climate response [*Toohey et al*., 2011].

[6] The most recent super-eruption, Toba, occurred about 74,000 years ago in Lake Toba, Sumatra, Indonesia. Given its antiquity, details for the Toba eruption are much more uncertain than for Pinatubo. The Toba eruption injected between one and three orders of magnitude more ash, dense rock [*Chesner and Luhr*, 2010; *Rose and Chesner*, 1987], and SO_2 [*Oppenheimer*, 2002] than Pinatubo, may have contributed to the onset of the following glacial cycle [*Rampino and Self*, 1992], and may have caused a bottleneck in human evolution [*Ambrose*, 1998; *Petraglia et al*., 2007; *Balter* 2010]. Initial modeling studies using bulk aerosol modules predicted 10 K cooling for about a decade and a temperature effect for a few decades [*Jones et al*., 2005; *Robock et al*., 2009], but a more recent study using a modal aerosol model found the temperature response to be three times weaker (−3.5 K globally) and shorter (9–10 years) due to aerosol growth [*Timmreck et al*., 2010].

[7] These studies confirm that the details of the aerosol size distribution can have enormous impacts on the temperature response after an eruption. In the present study, we perform simulations using a 3D microphysical sectional aerosol model that includes van der Waals forces in the coagulation scheme coupled to a general circulation model with prognostic chemistry (Whole Atmosphere Community Climate Model (WACCM)/Community Aerosol and Radiation Model for Atmospheres (CARMA)) to study the aerosol microphysics from volcanic eruptions spanning two orders of magnitude in SO_2 injection to the stratosphere (Pinatubo, ten times Pinatubo, and Toba). We provide a description of our model (section 2), the experimental design of our simulations (section 3), comparisons of our Pinatubo simulation to observations (section 4), the impact of volcanic eruption size on aerosol microphysics (section 5), a detailed study of the resulting size distributions to compare to modal models (section 6), and conclusions (section 7).

2. Model Description

[8] We use the WACCM version 3.1.9 tag 9 [*Garcia et al*., 2007] coupled with the CARMA [*Toon et al*., 1988]. This basic framework has been used to study sulfate nucleation [*English et al*., 2011], dust [*Su and Toon*, 2011], sea salt [*Fan and Toon*, 2011], noctilucent clouds [*Bardeen et al*., 2010], meteoric dust [*Neely et al*., 2011; *Bardeen et al*., 2008], black carbon [*Mills et al*., 2008; *Ross et al*., 2010], and stratospheric sulfur geoengineering [*English et al*., 2012]. A detailed description of this specific model is presented by *English et al*. [2011].

[9] For these simulations, we employ the standard spatial configuration of WACCM3, 4° latitude by 5° longitude horizontal resolution with 66 vertical levels from the surface

to the thermosphere (5.96×10^{-6} hPa, ~140 km), including 23 stratospheric levels between 1 and 100 hPa. A 63-species chemistry module is implemented that includes WACCM's standard 56-species chemical package (50 neutral species and reactions are listed in the auxiliary material of *Kinnison et al*. [2007] and six ion species and reactions are listed in *Marsh et al*. [2007]), and we have added seven sulfur-bearing gases: S, SO, SO_2, SO_3, $HOSO_2$, H_2SO_4, and OCS [*English et al*., 2011]. The model includes tropospheric emissions of carbonyl sulfide (OCS) and SO_2, two primary sulfur emissions of importance to the stratosphere. OCS is specified with a constant surface concentration of 510 pptv. Ground level emissions of SO_2 are specified from a two-dimensional monthly mean surface emissions dataset [*Lamarque et al*., 2010; *Smith et al*., 2011]. The model calculates prognostic OH concentrations based on production and loss chemistry for several species [*Kinnison et al*., 2007; *English et al*., 2011], which is useful because OH is limited after large eruptions, reducing the conversion rate of SO_2 to H_2SO_4 [*Bekki*, 1995]. Heterogeneous chemistry on sulfate aerosols is linked to CARMA aerosol surface area calculated from each timestep. However, photolysis rate calculations do not take the stratospheric aerosol optical depth (AOD) into account. Wet deposition for all constituents (including the aerosol bins from CARMA) is calculated using WACCM's existing techniques [*Barth et al*., 2000]. All of the aerosol bins are assumed to have a constant 0.3 solubility parameter. WACCM treats dry deposition of gases [*Barth et al*., 2000], while dry deposition of aerosols is not considered in our simulations.

[10] We specify 42 sulfuric acid mass bins in CARMA with mass doubling between bins. The model transports particle number for each mass bin and uses the *Lin and Rood* [1996] advection scheme to accurately treat advection on the size grid. Mass and number are conserved to machine accuracy in CARMA for microphysical processes that should conserve them. The bins are equivalent to particles with radius from 0.2 nm to 2.6 μm before water is added to them. Since the bins only carry sulfuric acid, the equivalent sulfate aerosol size (sulfuric acid plus water) is determined by the technique of *Tabazadeh et al*., [1997], which calculates equilibrium weight percent sulfuric acid as a function of temperature and water activity. Weight percent sulfuric acid is assumed to be independent of particle size. The particles are assumed to have spherical shape. Split-time stepping is enabled for nucleation and growth routines when sulfuric acid is supersaturated. Nucleation and growth are treated simultaneously in the model. If sulfuric acid gas concentrations become unstable (negative), the CARMA time step is retried with double the number of substeps. To improve substepping stability, we limited nucleation so that it did not consume more than 40% of the sulfuric acid available. Nucleation rates are calculated using the numerical scheme of *Zhao and Turco* [1995], which only considers binary homogeneous nucleation. Sulfuric acid surface tension is calculated using the constants from *Sabinina and Terpugow* [1935]. We did not include any other types of aerosols in CARMA, such as polar stratospheric clouds (these were treated using the WACCM parameterization), volcanic dust, or micrometeorites. Coagulation coefficients are calculated to include Brownian, convective, and gravitational effects, and a sticking coefficient of 1 is used, which assumes that all particles stick together upon colliding. A correction for the impact of interparticle Van der Waals forces on coagulation based on laboratory data [*Chan and Mozurkewich*, 2001] is included in some of our simulations, which increases the sticking coefficient to greater than 1 for smaller particles, and has been found to be important to accurately represent ambient stratospheric aerosol concentrations [*English et al*., 2011]. Sulfate aerosol growth and evaporation is calculated using sulfuric acid equilibrium vapor pressure over a binary solution computed from the method of *Ayers et al*. [1980] with a temperature correction by *Kulmala and Laaksonen* [1990] and thermodynamic constants from *Giauque et al*. [1960]. We assume a coefficient of unity for sulfuric acid uptake by aerosol particles, although there is considerable disagreement amongst laboratory measurements [*Hanson*, 2005]. Sedimentation is calculated based on particle size and density [*Lin and Rood*, 1996]. Aerosol radiative heating, which could impact stratospheric circulation especially for larger eruptions, is not coupled in this model version, but is planned for future versions of CAM and WACCM with CARMA.

3. Experimental Design

[11] To study the impacts of SO_2 injection magnitude on aerosol size distributions, we have completed simulations of eruptions spanning two orders of magnitude in stratospheric SO_2 injection: the 1991 eruption of Mount Pinatubo (10 Tg of S; "Pinatubo"), ten times Pinatubo (100 Tg S; "Pinatubo $\times 10$"), and the eruption of Toba 74,000 years ago (1000 Tg S; "Toba"). These injections are equivalent to 20 Tg SO_2 gas, 200 Tg SO_2 gas, and 2000 Tg SO_2 gas, respectively. To understand the impacts of van der Waal's forces on aerosol coagulation, for each eruption, we completed one simulation with and one simulation without ("no VW") the van der Waals correction for coagulation. For all eruptions, SO_2 gas is injected continuously over 48 h on 14 and 15 June of the first simulation year. Based on the approach of other models [*Timmreck et al*., 1999; *Weisenstein et al*., 2007], SO_2 is injected in the region 2°S to 14°N, 95°E to 115°E, corresponding with Total Ozone Mapping Spectrometer observations for 16 June 1991 [*Bluth et al*., 1992], and 15.1 to 28.5 km, corresponding with Microwave Limb Sounder (MLS) observations for 19 September 1991 [*Read et al*., 1993]. This approach allows for a realistic expansion of the volcanic cloud during the initial stages of the eruption, partially compensating for the lack of observationally driven meteorology in our simulations and the lack of aerosol heating in our model. In our 66-level model, the vertical profile of the injection is specified as a function of model level between 15.1 and 28.5 km with a peak at 21 km by the function:

$$Injection\ \ rate = \frac{3.52 \times 10^7}{abs(level - 43.5)}$$

where injection rate is in units of molecules of SO_2 cm^{-3} s^{-1}, *level* corresponds to model level number, which are numbered from the model top (1) to the model surface (66), and 43.5 is the level which corresponds to the peak injection altitude of 21 km. We assume that immediately after the eruption in June the SO_2 cloud peaked at 21 km. This altitude is slightly lower than found by LIDAR observations [*Antuña et al*., 2002] which observed a peak at 22 km in June (see Figure 5), and MLS observations [*Read et al*., 1993] which observed a peak at 25 km in September. These

differences in peak altitude may contribute to model biases for stratospheric lifetime and hemispheric transport. Also, our model's winds and circulation patterns were not constrained to observations for 1991 and 1992, which could contribute to differences between the model and observations. Our model does not have a QBO but instead predicts a prevailing easterly stratospheric circulation which happened to be consistent with the easterly phase of the QBO that was observed during the first year after the eruption of Mt. Pinatubo.

4. Pinatubo: Model Compared With Observations

[12] Model behavior can be studied by comparing our simulation of the eruption of Mount Pinatubo to available observations. The particle effective radius (R_{eff}), defined as the ratio of the third moment to the second moment of the aerosol size distribution, is a useful parameter to visualize the aerosol size distribution since it is the optically most important particle size. Prior to the simulated eruption, ambient stratospheric aerosol hydrated R_{eff} is approximately 0.2 μm in both regions analyzed (15 to 20°N and 35 to 45°N), comparable to observations (Figure 1). Immediately after the simulated eruption, R_{eff} temporarily drops due to new particle formation and then increases due to growth of existing particles and coagulation. R_{eff} continues to increase until its peak about 5 months after the eruption at about 0.72 μm at 15 to 20°N and 0.61 μm at 35 to 45°N for the simulation with the van der Waals coagulation. These values of R_{eff} are within the error bars of the observations which extend from 0.4 to >1.0 μm. R_{eff} from our model also compares well with observations at 68°N between 11.3 and 16.1 km in March 1992 (nine months after the eruption, approximately when particles reached peak size) from the Michelson interferometer for passive atmospheric sounding, balloon-borne version (MIPAS-B) [*Echle et al.*, 1998] (not shown). Our simulation with the van der Waals correction predicts R_{eff} to be 0.64 μm, and our simulation without the van der Waals correction predicts 0.62 μm; the values retrieved from MIPAS-B range from 0.53 to 1.19 μm. R_{eff} then slowly declines as the largest particles fall out of the stratosphere, shifting the size distribution to smaller sizes (Figure 1). R_{eff} is still slightly elevated above ambient values > 48 months after the eruption. The rate of decline in the model is faster than observations and is about 20% lower after about 2 to 4 years. It is likely that the simulated R_{eff} declines too quickly because aerosol heating was not included in the model. Aerosol heating would loft particles to higher altitudes, increase meridional transport to both hemispheres, and increase stratospheric lifetime, which would reduce the slope of the R_{eff} curve with time. This hypothesis, originally suggested by *Young et al.* [1994] and recently supported by *Timmreck and Graf* [2006] and *Aquila et al.* [2012], suggests that simulated aerosol mass burdens and AOD decline at a slower rate, more like observations, when aerosol heating is included. Another possible explanation is stratospheric circulation biases in the model. The WACCM3 model has been compared to observations, and biases attributed to gravity wave parameterization were found [*Richter et al.*, 2008]. In particular, the model does not include the QBO, which would slow transport of the volcanic cloud from the tropics to the poles [*Trepte and Hitchman*, 1992; *Thomas et al.*, 2009]. Additionally, aerosol radiative coupling would cause the surface to cool and the stratosphere to warm, possibly slowing the Brewer–Dobson circulation [*Garcia and Randel*, 2008].

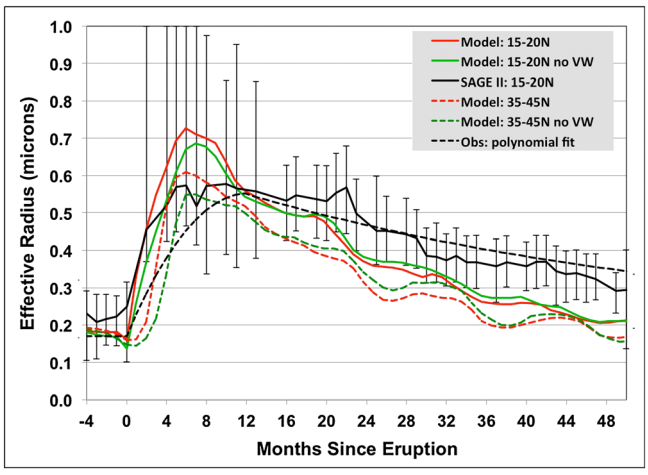

Figure 1. Time evolution of zonal-average R_{eff} compared in two regions: 15 to 20°N at 17 to 27 km (solid lines) and 35 to 45°N at 15 to 27 km (dotted lines). A second-order polynomial is fit to a compilation of observations mainly over California and Wyoming [*Russell et al.*, 1996] (dotted black line). SAGE II (solid black line) is a time series of retrieved column integrated R_{eff} in the 15 to 20°N latitude band [*Bauman et al.*, 2003]. Model results are monthly averages of hydrated sulfate R_{eff} for the simulation with the van der Waals coagulation correction (red lines) and without ("no VW"; green lines).

[13] Inclusion of van der Waals forces (red lines in Figure 1) increases "ambient" (prior to the eruption) and peak effective radii by about 10% compared to the simulation without van der Waals forces (green lines). It also accelerates the peak by about 1 month, due to an increase in the coagulation rate. Shortly after the peak size is reached, effective radii for the two simulations begin to converge. About 18 months after the eruption, R_{eff} becomes smaller for the simulation with van der Waals forces. This is due to the largest particles falling out of the stratosphere at a greater rate, due to enhanced coagulation.

[14] Next, we compare 525 nm AOD between 50 and 55°N for the model and observations. The simulation with van der Waals forces predicts zonal average to peak at 0.23 about nine months after the eruption (Figure 2). This peak AOD is about two orders of magnitude higher than ambient AOD in the stratosphere (~0.002) and on the order of the AOD persistently observed in the troposphere. Simulated AOD is generally within the range of error bars of the observations. As with the comparison of R_{eff}, the simulated AOD decreases too quickly and is lower than observations after about a year. Again, this too rapid decline in AOD is likely due to the lack of aerosol heating in the model, or errors in stratospheric circulation, particularly lack of the QBO in the model. AOD for the simulation with the van der Waals correction rises more quickly than the simulation without the van der Waals correction due to a faster coagulation rate to particles sizes that are optically significant. After about 6 months after the eruption, however, AOD for the simulation with the van der Waals is smaller due

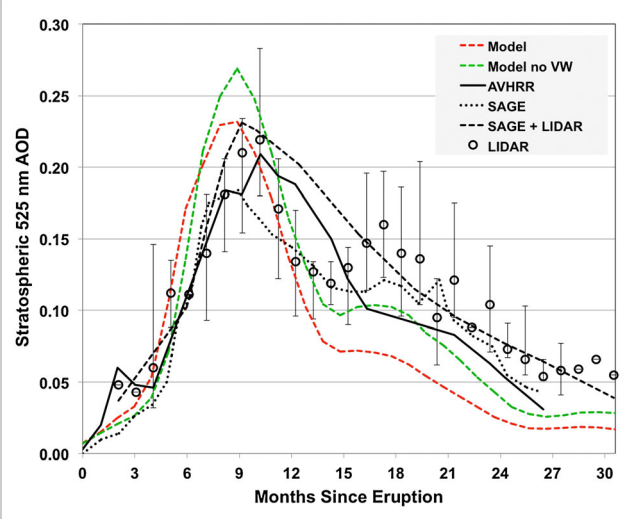

Figure 2. Time evolution of zonal-average stratospheric AOD in the visible at 50 to 55°N for the model (colored lines) compared to observations (black lines and circles). Observations are summarized by *Ansmann et al.* [1997]. AVHRR (solid line) is measured at 500 nm wavelength while SAGE II (dotted line) and LIDAR (circles) are at 525 nm. SAGE + LIDAR (dashed line) is SAGE data constrained to LIDAR observations. The LIDAR error bars are the standard deviation derived from the combined effect of signal noise, uncertainties in the atmospheric input parameters used in the determination, and the atmospheric variability. Modeled stratospheric AOD at 525 nm calculated from 1 to 300 hPa at 50 to 55°N at all longitudes for the simulation with the van der Waals coagulation correction (red lines) and without (green lines). Simulated extinction coefficients are calculated as a function of weight percent and wavelength using the refractive indices of *Palmer and Williams* [1975].

to the larger R_{eff} reducing extinction efficiency (extinction efficiency in the visible peaks at a particle radius of about 0.4 μm), and to larger particles falling out more quickly.

[15] A spatial comparison of stratospheric AOD at two wavelengths between the simulation with van der Waals forces and observations (Figure 3) shows that both the model and the observations have the highest AOD near the latitude of the eruption about 3 months after the eruption, and later a second peak in the Northern Hemisphere mid- to high latitudes about 9 months after the eruption as the cloud evolved and traveled towards the poles. At the equator, the magnitude of AOD in the visible (0.4) is consistent for both the model at 525 nm and the Advanced High Resolution Radiometer (AVHRR) data at 500 nm. The model is higher than SAGE II at both wavelengths. It is possible that AOD near the equator is enhanced in our model due to errors in stratospheric circulation, as the volcanic cloud did not travel to the Southern Hemisphere as observed. Given the bias is larger at 1024 nm, it is also possible that the simulated aerosol particles are too big. Another possibility is that our model does not treat volcanic ash. Ash particles, which were also injected into the stratosphere by the Mt. Pinatubo eruption, are relatively large and would remove some sulfate from the stratosphere in the first weeks after the eruption. Study of ash after Pinatubo reveals conflicting results. Some modeling studies suggest that the impact of ash on stratospheric AOD is minimal [*Niemeier et al.*, 2009], while observations of large dust particles in the Arctic months after the Pinatubo eruption suggest significant radiative heating due to the dust [*Pueschel et al.*, 1994]. There are also considerable differences between the AVHRR and SAGE II measurements, with SAGE II usually reporting lower peak AOD (Figures 2 and 3). *Russell et al.* [1996] concluded that most of the discrepancy is due to the evolution of particle size distribution combined with the wavelength differences of the instruments (AVHRR is measured at 500 nm and SAGE II at 525 nm). It is also possible that the differences between SAGE II and AVHRR are due to errors in the retrievals. AVHRR measures the column optical depth; significant uncertainty is introduced in stratospheric optical depth based on assumptions of the tropospheric component to subtract. SAGE II was unable to measure optical depths above 0.15 due to extinction of the signal along the limb path length, and while a correction was made by assuming extinction below the level of saturation was 80% of that measured before saturation [*Russell et al.*, 1996], measurement error was possible.

[16] Comparing zonal distribution of AOD, the model predicts a more pronounced hemispheric asymmetry than both AVHRR and SAGE II (Figure 3). The model overpredicts the peak in the Northern Hemisphere between 40°N and 60°N (this is also illustrated in Figure 2, where the simulated peak AOD is 0.23, AVHRR peaks at 0.20, and SAGE II peaks at 0.18), and underpredicts the peak in the Southern Hemisphere. The discrepancy in the Southern Hemisphere is more clearly illustrated by a comparison of zonal-average AOD between the model and AVHRR (Figure 4). While the simulated peak AOD is generally within 10% of the observations, observed AOD is significantly higher in the Southern Hemisphere. There are several possible explanations for these discrepancies. We have already mentioned the effects of aerosol heating and QBO which are not included in our model. Additionally, the eruption of Cerro Hudson in Chile, which is not included in the model, could be contributing to the bias. In September and October in the Southern Hemisphere mid- and high latitudes, observed AOD is about three times higher than the simulation (0.15 versus 0.05, respectively). Cerro Hudson's main eruption from 12–15 August in 1991 released slightly less than 1 Tg S up to 18 km altitude [*Pitts and Thomason*, 1993] and would have contributed to AOD in the Southern Hemisphere. Since aerosol from the El Chichon eruption (17°N) did not travel to the Southern Hemisphere even though its latitude is similar to that of Pinatubo, it is clear that the perturbed AOD in the Southern Hemisphere after Pinatubo was due to stratospheric circulation that year, the eruption of Cerro Hudson, or a contribution from both.

[17] The vertical distribution of 1 μm extinction with time at 18°N for the simulation with van der Waals correction peaks at about 22 km altitude during the first few months after the eruption, comparable to LIDAR observations (Figure 5), but the magnitude is about 50% too high (0.03 km^{-1} for the model and 0.02 km^{-1} for the observations. This bias may be due to the lack of aerosol heating or the lack of QBO in the model, which would disperse the volcanic cloud away from the latitude of LIDAR observations, reducing extinction. Also,

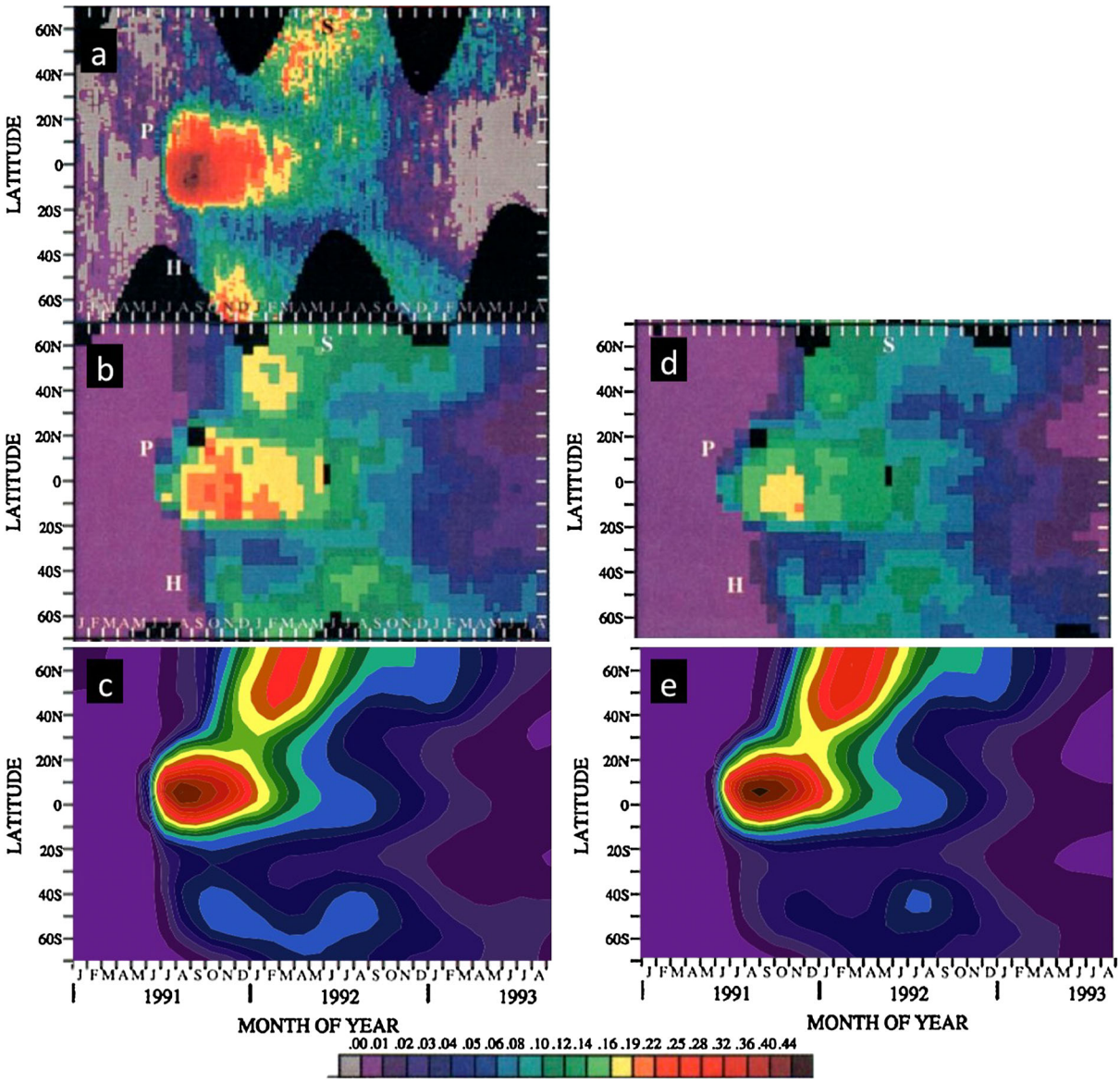

Figure 3. Spatial and temporal evolution of stratospheric AOD for the model and observations. (a) AVHRR at 500 nm (b) SAGE II at 525 nm (c) Model at 525 nm (d) SAGE II at 1024 nm (e) Model at 1024 nm. Observations summarized by *Russell et al*. [1996]. Modeled stratospheric AOD is calculated for the simulation with the van der Waals coagulation correction. Simulated extinction coefficients are calculated as a function of weight percent and wavelength using the refractive indices of *Palmer and Williams* [1975].

the model peak descends too rapidly with time. This, too, is likely due to the lack of aerosol heating in the model, which would loft the aerosol and prolong its stratospheric lifetime. Measurement error is also possible, as the LIDAR does not directly measure extinction and the conversion depends on assumptions of particle size and refractive index.

[18] Tropical sulfate burdens in the stratosphere peak about three months after the eruption (Figure 6a), consistent with the observations and the *e*-folding time for SO_2. Burdens peak at 18 Tg H_2SO_4 for the simulation with the van der Waals correction (Figure 6a), which is roughly two orders of magnitude higher than the stratospheric burden at ambient conditions, and within the range of CLAES observations [*Mergenthaler et al*., 1995] but lower than the High resolution Infrared Radiation Sounder (HIRS) [*Baran and Foot*, 1994]. The model also predicts higher burdens than HIRS globally (Figure 6b), as well as calculations using SAGE II observations [*McCormick and Veiga*, 1992], which estimated 20 to 30 Tg of aerosol (15 to 22 Tg H_2SO_4 assuming 75 weight percent H_2SO_4). There are considerable differences between the observations, so it is unclear whether the model has a bias. If the modeled burdens are too high, it may be due to the lack of QBO or errors with the Brewer–Dobson circulation, or errors with SO_2 injection magnitude. Regardless, simulated aerosol burdens decrease faster than HIRS and CLAES observations as well as LIDAR observations [*Ansmann et al*., 1997]. Recall that simulated tropical R_{eff} (Figure 1) and tropical AOD (Figure 3) also decreased more rapidly than observations. Again, the more rapid modeled decline than observed is likely due to the lack of aerosol

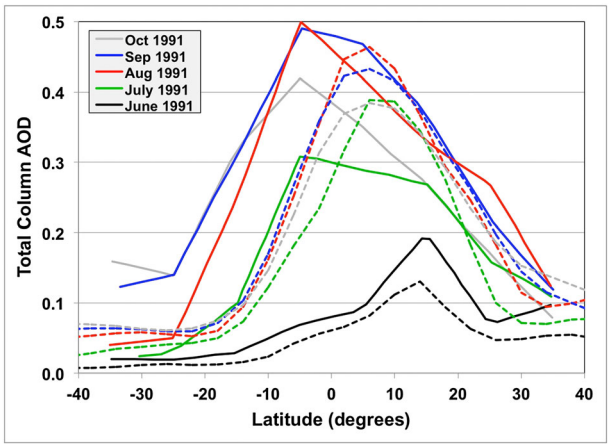

Figure 4. Monthly evolution of zonally average AOD compared to observations. Observations (solid lines) are total column AVHRR measurements of AOD at 500 nm summarized by *Minnis et al*. [1993]. Simulation (dotted lines) use monthly zonal averages of total column AOD at 525 nm for the simulation with the van der Waals coagulation correction. Simulated extinction coefficients are calculated as a function of weight percent and wavelength using the refractive indices of *Palmer and Williams* [1975].

heating in the model or errors in stratospheric circulation, particularly lack of the QBO in the model.

[19] The simulated eruption of Mount Pinatubo perturbs not only the stratospheric burden but tropospheric sulfate as well (Figure 7a, green lines). Earth's tropospheric burden has an annual cycle that is primarily controlled by the balance between sources (sulfur emissions) and losses (rainout), and in a typical year the model predicts a peak tropospheric burden of about 0.4 Tg S. However, this peak was perturbed by about 1 Tg S in the year following the eruption by sedimenting aerosols from the stratosphere at high latitudes [*Pueschel et al*., 1994]. An increase of large aerosols was measured in the upper troposphere after the eruption of Mount Pinatubo [*Ansmann et al*., 1993]. It is unclear whether these large aerosols impacted cirrus clouds; some observational analyses suggest that Pinatubo perturbed cirrus clouds [*Sassen et al*., 1995; *Minnis et al*., 1993; *Ackerman and Strabala*, 1994], while others suggest Pinatubo did not have an effect [*Luo et al*., 1997]. It is also possible that El Niño contributed to the change in cirrus properties that year [*Song et al*., 1996], but other analyses suggest El Niño was insignificant compared to the effects of Mt. Pinatubo [*Wang et al*., 1995]. *Lohmann et al*. [2003] conducted sensitivity studies using the ECHAM5 model and found Pinatubo to impact cirrus if a monomodal aerosol distribution was prescribed, but not if a bimodal distribution was prescribed. After a larger eruption such as Toba, tropospheric burdens are predicted to increase several orders of magnitude higher than after Pinatubo (Figure 7b), so more work should be done to understand the impacts a large volcanic eruption or a super-eruption may have on tropospheric clouds or chemistry.

5. Microphysics of Volcanic Clouds From Eruptions Larger than Pinatubo

[20] Here, we compare three volcanic simulations with the van der Waals coagulation using injections just described for Pinatubo, 10 times the Pinatubo injection, and 100 times the Pinatubo injection (which we refer to as the Toba injection). The globally averaged sulfate burdens peak at about 8 Tg S after Pinatubo, 74 Tg S after Pinatubo ×10, and 400 Tg S after Toba (Figure 8a). Toba burdens are 50 times higher than Pinatubo, despite 100 times SO_2 injection, due to faster sedimentation of larger particles. Globally averaged R_{eff} normalized by surface area in each grid box peaks at about 0.45 μm after Pinatubo, 1.1 μm after Pinatubo ×10, and 1.9 μm after Toba (Figure 8b). This change in R_{eff} has large implications for radiative forcing, as mass extinction

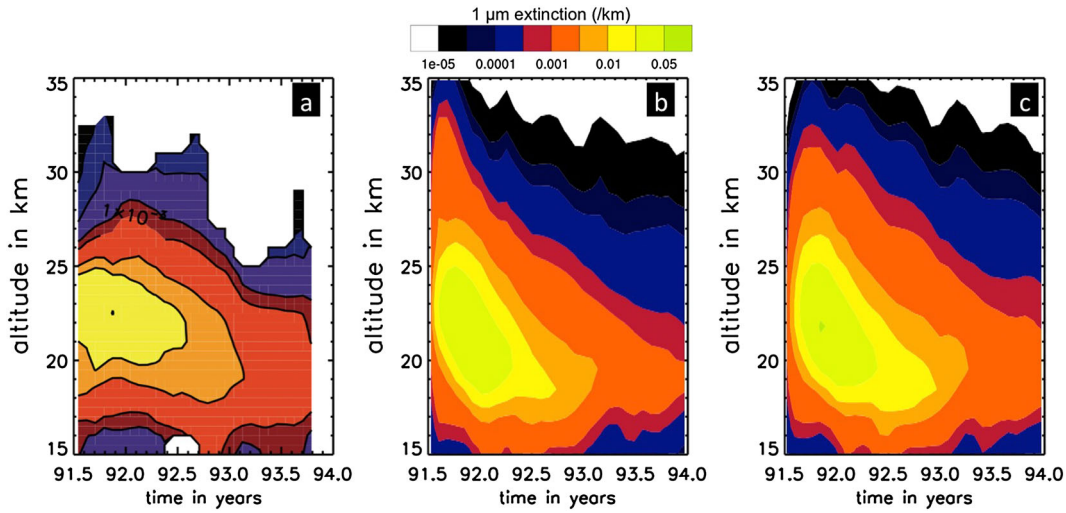

Figure 5. Vertical contour plots of zonal-average aerosol extinction for 2.5 years after the June 1991 Pinatubo eruption. (a) Observations at Mauna Loa and Camaguey derived from 1 μm LIDAR measurements [*Antuna et al*., 2002] compiled by *Heckendorn et al*. [2009].(b) Simulated 1024 nm extinction at 18°N for the simulation with van der Waals coagulation correction and (c) the simulation without van der Waals coagulation correction. Simulated extinction coefficients are calculated as a function of weight percent and wavelength using the refractive indices of *Palmer and Williams* [1975].

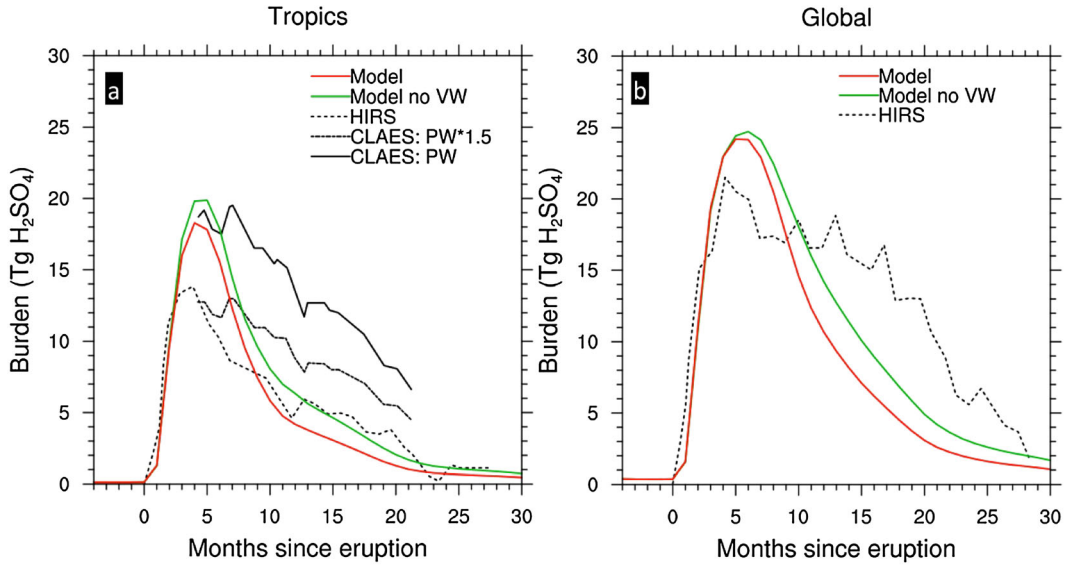

Figure 6. Time evolution of aerosol burden (Tg H_2SO_4) above 121 hPa for the model and observations in two regions: (a) "Tropics" (between 20°S and 20°N) and (b) "Global" (between 80°S and 80°N). Simulations with the van der Waals correction (red lines) and without (green lines) are compared. The Cryogenic Limb Array Etalon Spectromer (CLAES) was used to provide two estimates based on two different indices of refraction: those from *Palmer and Williams* [1975] (PW) and multiplying the PW imaginary component by 1.5 (PW*1.5) [*Mergenthaler et al.*, 1995]. The high-resolution infrared radiation sounder (HIRS) measurements include tropospheric aerosol [*Baran and Foot*, 1994].

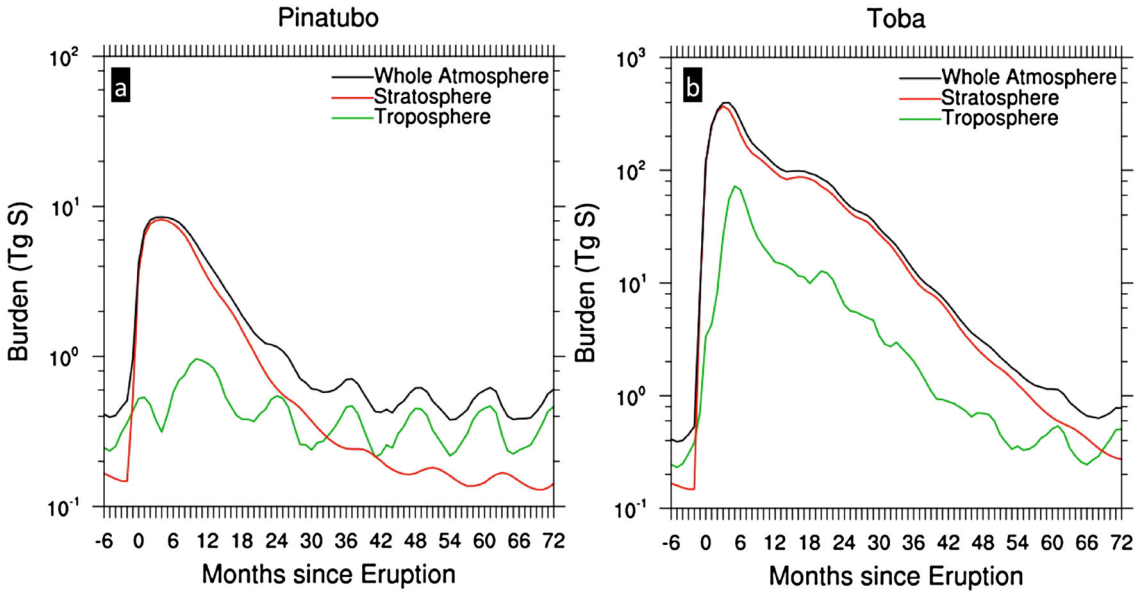

Figure 7. Evolution of sulfate burden (Tg S) after (a) the Pinatubo eruption and (b) the Toba eruption for the simulations with the van der Waals coagulation correction. To separate tropospheric from stratospheric burdens, the tropopause was defined based on a lapse rate definition modified from the World Meteorological Organization [*WMO*, 1957]. Here, the tropopause is identified as the lowest level at which the lapse rate is closer to zero than -4 K km^{-1} at that level and the level above it. If the lapse rate at the level above the current level was +2 K km^{-1} or more, the current level was flagged as the tropopause regardless of whether the current level lapse rate is less than -4 K km^{-1}. The search began above the boundary layer to avoid designation of boundary layer inversions as the tropopause. Tropopause levels were constrained to be between the pressures 85 to 433 hPa.

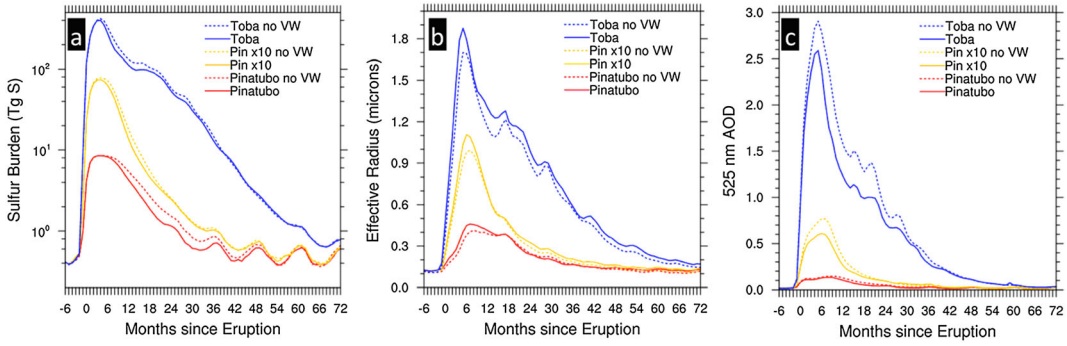

Figure 8. Temporal evolution of global-average aerosol for the six simulations: (a) burdens (Tg S), (b) 525 nm AOD, and (c) R_{eff}. R_{eff} is weighted by dividing the aerosol surface area in each grid box by the total vertically integrated surface area to normalize by the amount of aerosol in each grid box. Surface area was chosen to provide a consistent weighting to the denominator of the definition of effective radius. Note R_{eff} and AOD are on a linear y-axis but burdens are on a log y-axis.

efficiency at 525 nm is about five times higher for sulfate aerosols of 0.45 nm radii compared to those of 1.9 μm radii. This change in efficiency is illustrated in a comparison of globally averaged 525 nm AOD (Figure 8c), which is only 20 times higher after Toba than after Pinatubo (2.6 versus 0.13, respectively), due to the combined effects of faster sedimentation and lower extinction efficiency for larger particles. For these same reasons, larger volcanic eruption clouds generally take less time to reach peak values of R_{eff} and AOD. Global sulfur burdens reach peak values 5 months after the simulated Pinatubo eruption, 4 months after Pinatubo ×10, and 4 months after Toba. R_{eff} and 525 nm AOD peak 8 months after Pinatubo, 6 months after Pinatubo ×10, and 4 months after the Toba eruption. The length of the radiative effect, based on the time that the globally averaged 525 nm AOD remains larger than 0.1 (Figure 8c), is about 1 year after a simulated Pinatubo eruption, 2 years after Pinatubo ×10, and 4 years after a Toba eruption. In general, adding the van der Waals coagulation correction to the model predicts larger particles, and, as a result, lowers burdens and lowers 525 nm AOD. For the Toba eruption, the simulation with the van der Waals coagulation correction predicts roughly 10% larger particles, 10% lower burdens, and 20% lower AOD than the simulation without. Vertically, extinction initially peaks near the injection zone in the stratosphere between 10 and 100 hPa, then the peak descends into the troposphere as the particles grow and sediment (Figures 9a, 9b, and 9c). Immediately after the eruptions, 525 nm AOD increases near the equator due to aerosol nucleation near the injection zone. As the cloud spreads poleward, AOD and column mass increase until they reach a maximum several months later due to additional nucleation and condensational growth combined with a longer dynamical residence time of lower stratospheric air at higher latitudes compared to the tropics. The rate of vertical and horizontal spreading would likely be strongly modulated by radiative feedbacks not included in these simulations. The growth of particles over time is illustrated by plotting R_{eff} (Figure 10), where R_{eff} is highest at high latitudes and lower altitudes as the particles grow with time. While R_{eff} is largest near the poles for all eruptions, the altitude varies depending on the eruption. R_{eff} is largest at 100 hPa after the simulated Pinatubo eruption, 500 hPa after Pinatubo ×10, and near the surface after Toba. The increasing pressure for the maximum particle size reflects the faster falling rate of the aerosol particles for the larger eruptions.

[21] Comparing the Toba eruption using our sectional model with the van der Waals correction to that of a modal model without the van der Waals correction [*Timmreck et al.*, 2010], we predict larger zonal-average stratospheric effective radii in the lower stratosphere after the eruption (1.6 μm versus 1.1 μm) and near the earth's surface (2.5 μm versus 0.6 μm), smaller globally averaged peak 525 nm AOD (2.5 versus 4.0), and a longer radiative effect based on 525 nm AOD greater than 0.1 (4.1 years versus 3.5 years). There are several possible explanations for the differences in our simulations. We injected 1000 Tg S in our model, while *Timmreck et al.* [2010] injected 850 Tg S in their model. Our larger injection could account for some of the increase in R_{eff}, and if the particles got big enough, a reduction in 525 nm AOD. *Timmreck et al.* [2010] included aerosol heating in their model, which would disperse the cloud more quickly away from the injection zone, likely reducing R_{eff}, and if particle growth was sufficiently limited, increase AOD. Our model includes van der Waals forces in our coagulation scheme, while the model from *Timmreck et al.* [2010] does not. Indeed, our simulation without van der Waals correction predicts R_{eff} (1.3 μm versus 1.1 μm in the lower stratosphere) and 525 nm AOD (2.9 versus 4.0) closer to that from *Timmreck et al.* [2010] than our simulation with the van der Waals correction. Another possible factor in the difference between simulations is that our aerosol size distributions consist of an evolving mode peak radius as well as mode width. *Timmreck et al.* [2010], utilizing a two-moment modal model, prescribed a constant mode width, as do most modal models. Aerosol size distributions are discussed in more detail in the next section.

[22] Our simulations suggest that the climate effects from the Toba super-eruption may not have been as severe as originally suggested by simulations using bulk aerosol models [*Jones et al.*, 2005; *Robock et al.*, 2009] due to particle growth to large sizes, consistent with results originally postulated by *Pinto et al.* [1989] and recent results by *Timmreck et al.* [2010]. Our simulations do not include feedbacks with the land surface, but other climate simulations coupled to dynamic vegetation found insufficient feedbacks in

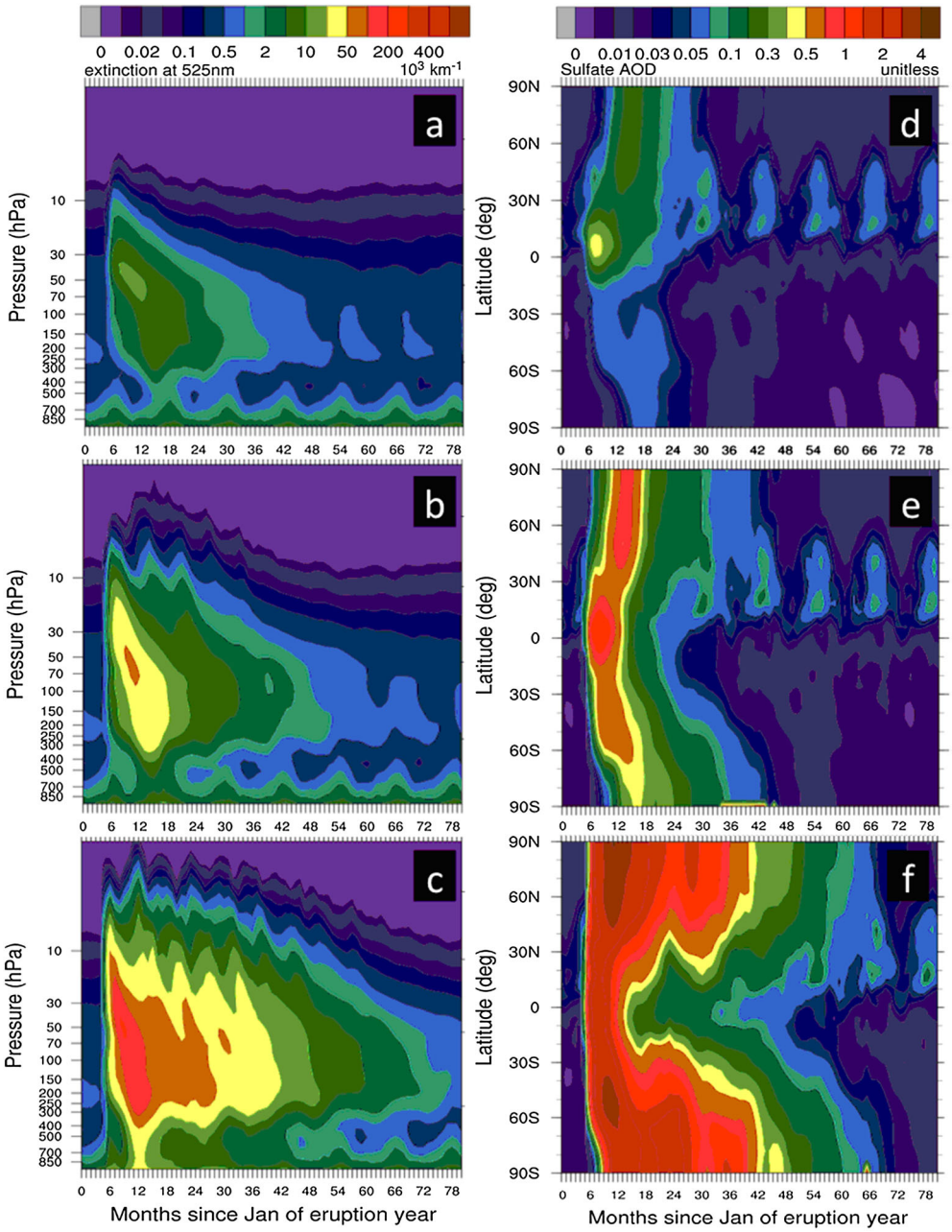

Figure 9. Vertical contour plots of global-average 525 nm extinction (times 10^3 km^{-1}) as a function of time for (a) simulated Pinatubo eruption, (b) simulated 10 times Pinatubo eruption, and (c) Simulated Toba eruption. Zonal average contour plots of 525 nm AOD as a function of time for (d) simulated Pinatubo eruption, (e) simulated 10 times Pinatubo eruption, and (f) simulated Toba eruption. All simulations include the van der Waals coagulation correction. Simulated extinction coefficients are calculated as a function of weight percent and wavelength using the refractive indices of *Palmer and Williams* [1975].

the land–atmosphere system to cause a sustained climate impact [*Robock et al.*, 2009]. As *Robock et al.* [2009] prescribed a smaller R_{eff} (0.4 μm dry R_{eff}) than predicted by our sectional model, it is likely the climate effect is even smaller than they postulated.

6. Aerosol Size Distribution Properties

[23] Our sectional model predicts significant shifts to the nucleation and accumulation modes after the simulated eruptions. In this section, we focus on evolution of the accumulation mode. Although the nucleation mode shifts significantly, the accumulation mode is the dominant contributor to mass extinction efficiency and aerosol burdens. Recall that various aerosol modules (bulk, modal, and sectional) predict varying radiative effects due in part to differences in R_{eff} which is strongly related to the accumulation mode. An analysis of monthly averaged aerosol size distributions after the simulated Pinatubo and Toba eruptions reveal large changes in aerosol size modes in the tropical tropopause region and high-latitude

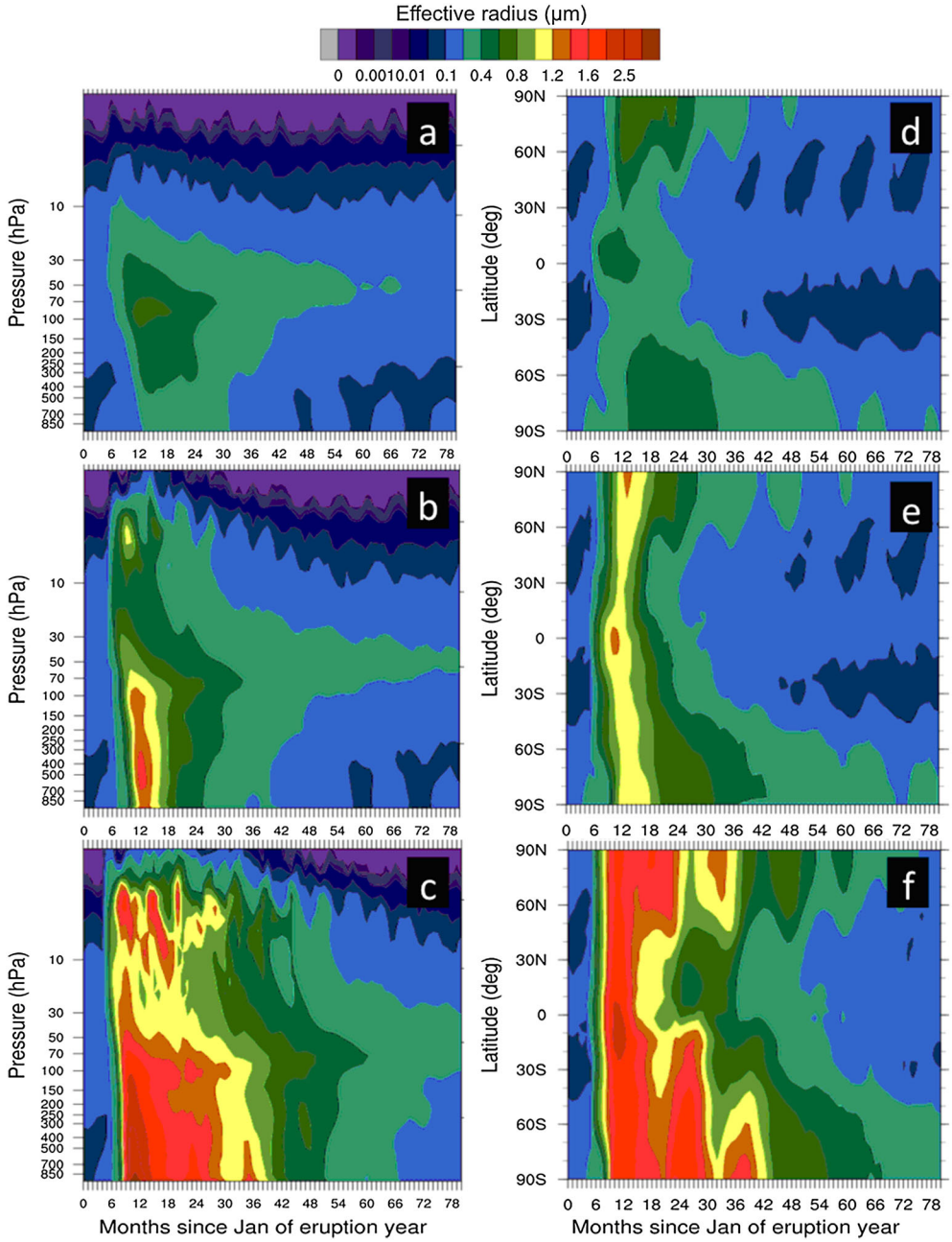

Figure 10. (a–c) Vertical contour plots of R_{eff} (um) as a function of time for (a) simulated Pinatubo eruption, (b) simulated ten times Pinatubo eruption, and (c) simulated Toba eruption. (d–f) Zonal average contour plots of R_{eff} as a function of time for (d) simulated Pinatubo eruption, (e) simulated 10 times Pinatubo eruption, and (f) simulated Toba eruption. R_{eff} is weighted by dividing the aerosol surface area in each grid box by the total vertically integrated surface area to normalize by the amount of aerosol in each grid box. Surface area was chosen to provide a consistent weighting to the denominator of the definition of R_{eff}. All simulations include the van der Waals coagulation correction. Simulated extinction coefficients are calculated as a function of weight percent and wavelength using the refractive indices of *Palmer and Williams* [1975].

troposphere and stratosphere (Figure 11). In the first few months after both simulated eruptions, there is a one to two order of magnitude increase in particle number in the tropical stratosphere due to nucleation (months 7 and 9 in Figures 11a and 11b). Particle growth and coagulation creates an accumulation mode that is defined by month 11 and reaches its peak size larger than 1 μm a month later, and then proceeds to decrease in size and number for the remainder of the 3 year period. In the high-latitude troposphere and stratosphere (Figures 11c and 11d), the aerosols have aged somewhat and have been transported to this region from the tropical stratosphere via the Brewer–Dobson circulation. The appearance of the accumulation mode particles is delayed compared to the tropical stratosphere, but the particles are larger, reflecting the additional time to grow. In the high-latitude stratosphere, the accumulation mode reaches its peak size about 15 months after the Pinatubo

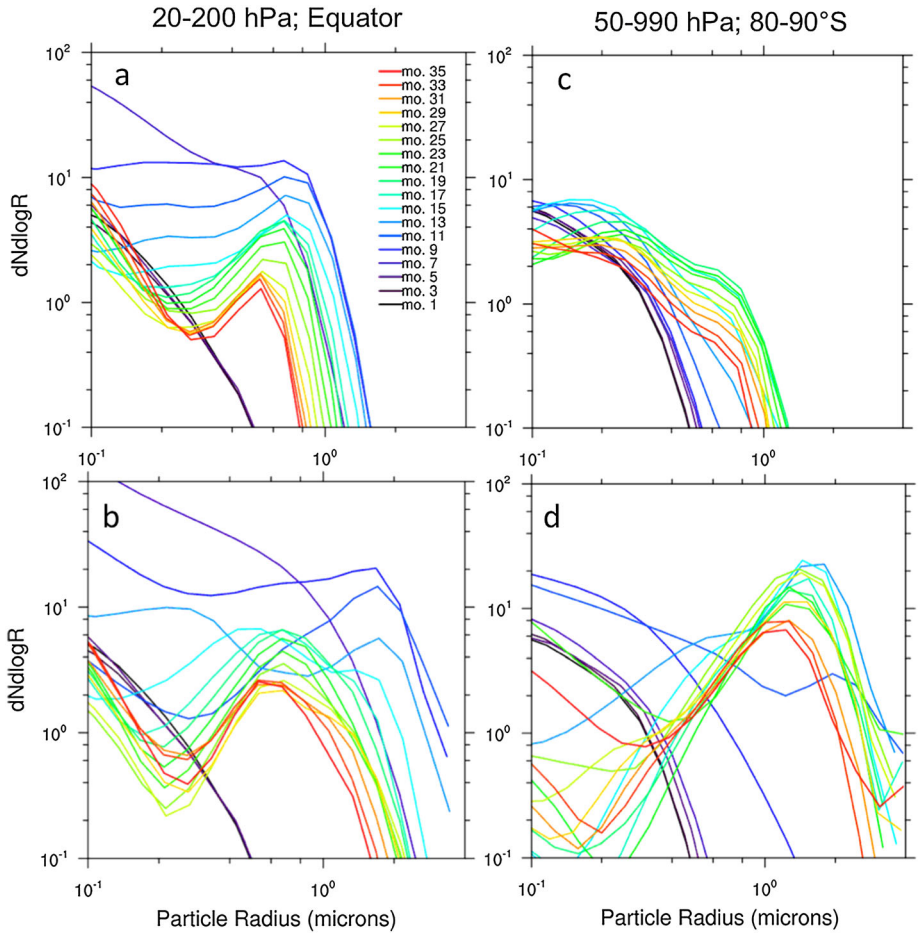

Figure 11. Evolving monthly average accumulation mode size distribution for Pinatubo (top row) and Toba (bottom row) every 2 months for 35 months. The eruption occurred in month 6. The regions analyzed were chosen to include the majority of the volcanic cloud for both eruptions.

eruption (month 21 in Figure 11c) and about 7 months after the Toba eruption (month 13 in Figure 11d). In both regions, the particles at the large end of the accumulation mode disappear more quickly than those at the small end of the accumulation mode due to the faster sedimentation of the largest particles. The details of this evolving aerosol size distribution can have significant impacts on radiative forcing, as aerosol mass extinction efficiency is strongly related to particle radius. Aerosol mass extinction efficiency for 525 nm radiation peaks at about 0.4 μm particle radius and for 1024 nm radiation peaks at about 0.8 μm radius. When particles are larger than the radius of maximum mass extinction, their radiative forcing is less efficient. Hence, large eruptions, with their large particles, can be self-limiting.

[24] The evolving size distributions predicted by our sectional model are complex and would be difficult to accurately prescribe in bulk aerosol or modal models. To assist with comparison to modal models, we calculate accumulation mode peak size and width from our sectional model by finding the mode width that most closely resembles our size distributions, assuming a lognormal shape. Mode width is found by finding the mode width of a lognormal distribution with the smallest difference from our sectional model. Difference is calculated by summing fractional errors at each bin on the large half of the distribution (from the mode peak to the largest bin) and finding the mode width with the smallest error. Calculations begin with the first month containing an accumulation mode in that region, which ranged from zero to three months after the eruption. These calculations have been completed for the three simulated eruptions over time. In the tropical stratosphere (Figure 12a), the mode peak size is predicted to reach 0.69 μm after Pinatubo, 1.3 μm after Pinatubo ×10, and 1.7 μm after Toba, afterwards decreasing within a few months to about 0.5 μm as the particles are transported to higher latitudes via the Brewer–Dobson circulation. In the high-latitude troposphere and stratosphere (Figure 12b), there is a longer time lag to reach mode peak size (12 months after the Pinatubo eruption, 6 months after the Pinatubo ×10 eruption, and 4 months after Toba), but the peak size is larger except for Pinatubo (2.0 μm for Toba, 1.5 μm for Pinatubo ×10, and 0.32 μm for Pinatubo). Due to a relatively longer aerosol lifetime in the troposphere and stratosphere, the rate of decline is slower in the high latitudes, with mode peak size still declining after 5 years for the eruptions larger than Pinatubo. Mode widths are generally more stable with time than R_{eff}, but vary significantly with eruption size. In the tropical stratosphere, the Pinatubo mode width is about 1.2 and Pinatubo ×10 is about 1.3. Mode width is about 1.3 for the first 6 months after the simulated Toba eruption, then jumps to 1.6 as the accumulation mode broadens and the mode

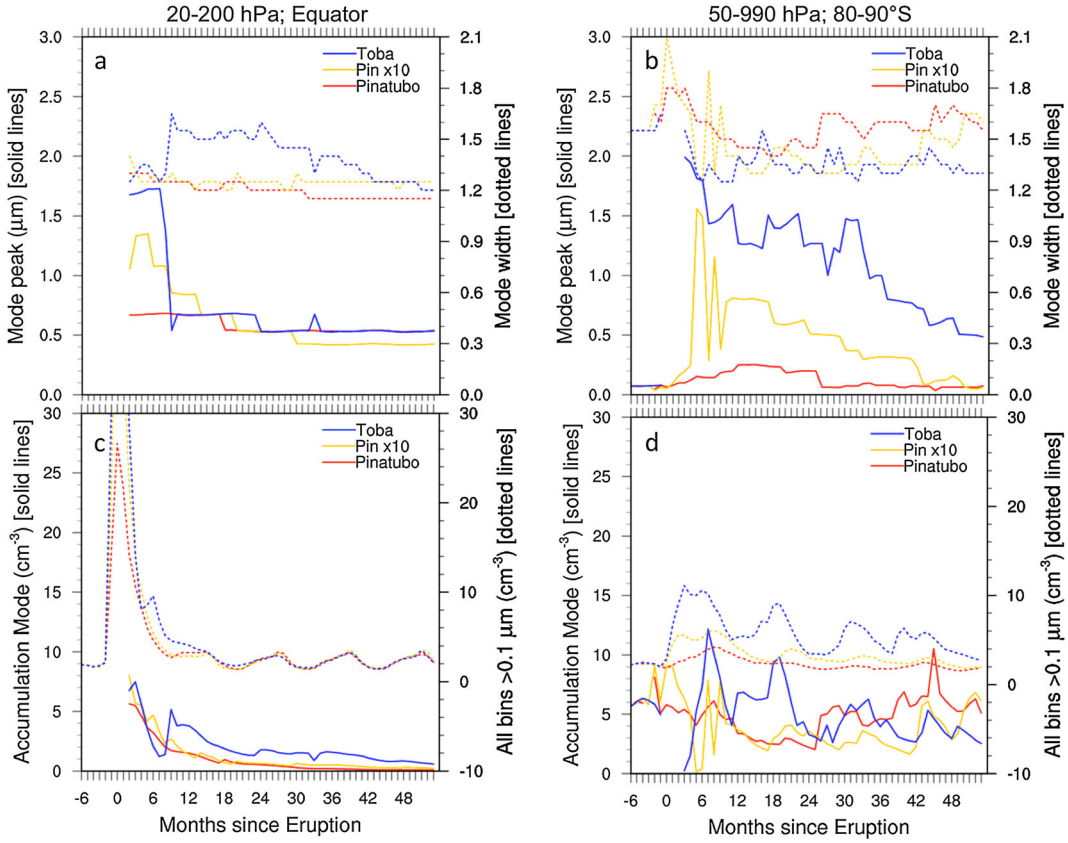

Figure 12. (a–b) Simulated monthly average peak mode radius (μm) and mode width (assuming a lognormal mode) for Pinatubo, Pinatubo ×10, and Toba eruptions over time in two regions. Calculations were made assuming a lognormal shape. Mode peak is found by the searching for the first maxima in dndlogr smaller than the largest bin. Mode width is found by finding the mode width of a lognormal distribution with the smallest difference from our sectional model. Difference is calculated by summing fractional errors at each bin on the large half of the distribution (from the mode peak to the largest bin) and finding the mode width with the smallest error. Gaps occur when the accumulation mode did not have a peak. (c–d) Simulated monthly average aerosol number (cm^{-3}) in the accumulation mode (solid lines) and across all bins > 0.1 μm (dashed lines). Accumulation mode number is found by adding up all bins from the mode peak to the largest bin and doubling it, because overlap between the accumulation mode and nucleation mode made determination of aerosol number difficult at sizes smaller than the mode peak. Gaps occur when the accumulation mode did not have a peak.

peak gets smaller, then slowly declines back to 1.2. In the high-latitude troposphere and stratosphere, mode width ranges from 1.4 to 1.8 after the Pinatubo eruption, 1.3 to 1.9 after Pinatubo ×10, and 1.3 to 1.5 after Toba. The mode width broadening is due to condensational growth of excess H_2SO_4 onto pre-existing particles, particularly in the tropics. The mode peak and mode width curves would likely be smoother with higher bin resolution (our model had six bins between 0.5 and 2.0 μm for these simulations). Also, it is not clear how much mode peak or widths predicted by our sectional modal would change if our model included aerosol heating or QBO. Aerosol number in the accumulation mode in the tropical stratosphere (Figure 12c, solid lines) increases about a month after the eruption due to coagulation and growth of nucleation mode particles, then declines due to coagulation within the accumulation mode, sedimentation, and transport to high latitudes. In the high-latitude troposphere and stratosphere (Figure 12d, solid lines), aerosol number in the accumulation mode increases about 6 months after the eruption due to transport from the tropics. In both regions for all eruptions, there is significant variation in aerosol number in the accumulation mode with time. The perturbations generally correspond with times when the nucleation mode is shifting to the accumulation mode (see Figure 11). During these times, the shape of the accumulation mode is not well defined due to overlap with the nucleation mode. It is difficult to compute aerosol number in the accumulation mode due to this overlap. Therefore, we computed aerosol number on the large size of the mode peak only and doubled the number. This may introduce errors if the mode is not symmetric. When computing aerosol number at all sizes greater than 0.1 μm (Figures 12c and 12d, dotted lines), the curves are smoother with time.

[25] *Timmreck et al.* [2010] prescribed a mode width of 1.2 for their Toba simulation, which is close to the mode width predicted by our sectional model in the tropical stratosphere during the first 6 months after the eruption, but in the low end of the range of mode widths found when

analyzing a broader spatial and temporal range (1.2 to 1.6). It is unclear how much this would impact their results. In the stratosphere, the large end of the size distribution can significantly impact sedimentation rates and differences in mode width significantly impacted stratospheric aerosol properties when comparing modal and sectional models [*Weisenstein et al*., 2007]. In an intercomparison study, *Weisenstein et al*. [2007] found sectional models to predict larger stratospheric aerosols after Pinatubo than modal models, and sectional models compared better to observations. *Kokkola et al*. [2009] completed an intercomparison between microphysical and sectional versions of the ECHAM model and found significant differences in the evolution of stratospheric aerosol size distributions, with differences between modal and sectional models increasing with increasing SO_2 injection rate. *Mann et al*. [2012] found significant changes in simulated aerosol mixing ratios and number concentrations in the lower troposphere when modifying mode widths and found that changing the mode width from 1.59 to 1.4 significantly improved a comparison of their modal model to observations of different aerosols. Future modeling studies should include aerosol radiative feedbacks, van der Waals forces in the coagulation scheme, and sectional bin representation for a more comprehensive understanding of aerosol evolution after volcanic eruptions.

7. Conclusions

[26] Simulations of the 1991 eruption of Mount Pinatubo using a 3D microphysical sectional aerosol model coupled to a whole atmosphere model (WACCM/CARMA) predict the magnitude and timing of peak R_{eff}, 525 nm AOD, and tropical burden to be within the range of available observations. The model predicts zonal-average stratospheric R_{eff} at 15°N to increase from 0.19 μm at ambient conditions to 0.72 μm six months after the eruption. The stratospheric aerosol perturbations as defined by changes in R_{eff}, 525 nm AOD, and burden decrease more quickly in the model than observed by AVHRR, SAGE II, HIRS, and CLAES, which is likely due to lack of aerosol heating in the model. Heating would increase aerosol lofting to higher altitudes, hemispheric transport, and stratospheric lifetime. This hypothesis is supported by simulations with and without aerosol heating by *Young et al*. [1994], *Timmreck and Graf* [2006] and *Aquila et al*. [2012]. In the mid- and high-latitude Southern Hemisphere, the simulated 525 nm AOD is about one-third that of observations 3 months after the eruption. This difference, in addition to the lack of aerosol heating in the model which would increase hemispheric transport, may also be due to the August eruption of Cerro Hudson in Chile, which is not included in the model. Finally, some discrepancy between the model and observation may also be caused by differences in meteorology (QBO and Brewer–Dobson circulation), as the model was run freely and not constrained to the actual wind patterns present during the 1991 eruption, although in 1991, the QBO was in an easterly phase, and the model predicts constant easterlies.

[27] Volcanic eruptions with increasing SO_2 injection size are predicted to have self-limiting effects due to particle growth, as originally postulated by *Pinto et al*. [1989] and supported by *Timmreck et al*. [2010]. Our simulations predict globally averaged R_{eff} between 1 and 200 hPa to peak at about 0.45 μm after Pinatubo and 1.9 μm after Toba. Peak burdens after Toba are 50 times higher than after Pinatubo, despite 100 times SO_2 injection size. 525 nm AOD is limited further, due to the combined effect of faster sedimentation rates and lower extinction efficiency per unit mass. Globally averaged 525 nm AOD after Toba is only 20 times higher than after Pinatubo (2.6 versus 0.13, respectively).

[28] The aerosol size distributions in our sectional model are predicted to vary spatially and temporally after simulated eruptions. We fit lognormal size distributions to modeled size distributions to better understand how a model using a modal representation rather than the sectional representation we used might track the volcanic cloud size distribution. In the tropical stratosphere, the simulated mode peak size reached 0.69 μm after Pinatubo, 1.26 μm after Pinatubo ×10, and 1.75 μm after Toba. Mode widths are generally more stable with time, but vary significantly with eruption size, altitude, and latitude. Mode widths range from 1.2 to 1.9 and are generally wider with larger eruptions, but not always. To date, bulk aerosol studies [*Robock et al*., 2009] and modal aerosol studies [*Timmreck et al*., 2010] of Toba prescribe a constant mode width. It is unclear how much error using a fixed mode width would introduce. Intercomparison studies have found modal models to have biases in stratospheric aerosol properties due to errors in mode widths [*Weisenstein et al*., 2007] and found that changing the mode width improved comparisons to surface aerosol [*Mann et al*., 2012].

[29] Adding van der Waals forces to our coagulation scheme increases the growth rate of stratospheric aerosols, with R_{eff}, 525 nm AOD, and burdens reaching peak values more quickly, increasing the peak R_{eff}, and decreasing peak 525 nm AOD due to the lower extinction efficiency per unit mass for larger particles. Due to the uncertainty of observations after Pinatubo, it is unclear whether simulations that include van der Waals forces better match observations after a volcanic eruption. However, simulations with van der Waals forces have been found to better match aircraft observations of ambient stratospheric aerosol number concentration [*English et al*., 2011], and laboratory measurements have suggested the importance of van der Waals forces for coagulation rates of sulfate aerosols [*Chan and Mozurkewich*, 2001]. Sulfate aerosol models should include van der Waals forces in their coagulation schemes, especially when studying the stratosphere or other applications where sedimentation rates are very sensitive to aerosol size distribution. Future modeling studies should include aerosol radiative feedbacks, the presence of a QBO, van der Waals forces in the coagulation scheme, and sectional bin representation for a more comprehensive understanding of aerosol evolution after volcanic eruptions.

[30] **Acknowledgments.** We thank Charles Bardeen for help coupling CARMA and WACCM. This work was supported by NSF Award ATM-0856007, NASA Award NNX09AK71G, and NASA GSRP Fellowship NNX-09AM38H. NCAR is sponsored by the National Science Foundation.

References

Ackerman, S. A., and K. I. Strabala (1994), Satellite remote sensing of H_2SO_4 aerosol using the 8- to 12-μm window region: Application to Mount Pinatubo, *J. Geophys. Res.*, *99*(D9), 18,639–18,649, doi:10.1029/94JD01331.

Ambrose, S. H. (1998), Late Pleistocene human population bottlenecks, volcanic winter, and differentiation of modern humans, *J. Hum. Evol.*, *34*, 623–651.

Ansmann, A., U. Wandinger, and C. Weitkamp (1993), One-year observations of Mount-Pinatubo aerosol with an advanced Raman lidar over Germany at 53.5° N, *Geophys. Res. Lett.*, *20*(8), 711–714, doi:10.1029/93GL00266.

Ansmann, A., I. Mattis, U. Wandinger, F. Wagner, J. Reichardt, and T. Deshler (1997), Evolution of the Pinatubo aerosol: Raman Lidar observations of particle optical depth, effective radius, mass, and surface area over Central Europe at 53.4°N, *J. Atmos. Sci.*, *54*, 2630–2641, doi:10.1175/1520-0469(1997)054<2630:EOTPAR>2.0.CO;2.

Antuña, J. C., A. Robock, G. L. Stenchikov, L. W. Thomason, and J. E. Barnes (2002), Lidar validation of SAGE II aerosol measurements after the 1991 Mount Pinatubo eruption. *J. Geophys. Res.*, *107* (D14), 4194, doi:10.1029/2001JD001441.

Aquila, V., L. D. Oman, R. S. Stolarski, P. R. Colarco, and P. A. Newman (2012), Dispersion of the volcanic sulfate cloud from a Mount Pinatubo–like eruption, *J. Geophys. Res.*, *117*, D06216, doi:10.1029/2011JD016968.

Ayers, G. P., R. W. Gillett, and J. L. Gras (1980), On the vapor-pressure of sulfuric acid, *Geophys. Res. Lett.*, *7*(6), 433–436.

Baldwin, M. P., et al. (2001), The Quasi-Biennial Oscillation, *Rev. Geophys.*, *39*, 179–229.

Balter, M. (2010), Of two minds about Toba's impact, *Science*, *327*, 1187–1188, doi:10.1126/science.327.5970.1187-a.

Baran, A. J., and J. S. Foot (1994), New application of the operational sounder HIRS in determining a climatology of sulphuric acid aerosol from the Pinatubo eruption, *J. Geophys. Res.*, *99*(D12), 25,673–25,679, doi:10.1029/94JD02044.

Bardeen, C. G., O. B. Toon, E. J. Jensen, D. R. Marsh, and V. L. Harvey (2008), Numerical simulations of the three-dimensional distribution of meteoric dust in the mesosphere and upper stratosphere, *J. Geophys. Res.*, *113*, D17202, doi 10.1029/2007jd009515.

Bardeen, C. G., O. B. Toon, E. J. Jensen, M. E. Hervig, C. E. Randall, S. Benze, D. R. Marsh, and A. Merkel (2010), Numerical simulations of the three-dimensional distribution of polar mesospheric clouds and comparisons with Cloud Imaging and Particle Size (CIPS) experiment and the Solar Occultation For Ice Experiment (SOFIE) observations, *J. Geophys. Res.*, *115*, D10204, doi:10.1029/2009JD012451.

Barth, M. C., P. J. Rasch, J. T. Kiehl, C. M. Benkovitz, and S. E. Schwartz (2000), Sulfur chemistry in the National Center for Atmospheric Research Community Climate Model: Description, evaluation, features, and sensitivity to aqueous chemistry, *J. Geophys. Res.-Atmos.*, *105*(D1), 1387–1415.

Bauman, J. J., P. B. Russell, M. A. Geller, and P. Hamill (2003), A stratospheric aerosol climatology from SAGE II and CLAES measurements: 2. Results and comparisons, 1984–1999, *J. Geophys. Res.*, *108*(D13), 4383, doi:10.1029/2002JD002993.

Bekki, S. (1995), Oxidation of volcanic SO_2: A sink for stratospheric OH and H_2O, *Geophys. Res. Lett.*, *22*(8), 913–916, doi:10.1029/95GL00534.

Bekki, S., and J. A. Pyle (1994), A two-dimensional modeling study of the volcanic eruption of Mount Pinatubo, *J. Geophys. Res.*, *99*(D9), 18,861–18,869, doi:10.1029/94JD00667.

Bluth, G. J. S., S. D. Doiron, C. C. Schnetzler, A. J. Krueger, and L. S. Walter (1992), Global tracking of the SO2 clouds from the June 1991 Mount Pinatubo eruptions, *Geophys. Res. Lett.*, *19*, 151–154.

Chan, T. W., and M. Mozurkewich (2001), Measurement of the coagulation rate constant for sulfuric acid particles as a function of particle size using tandem differential mobility analysis, *J. Aerosol Sci.*, *32*(3), 321–339.

Chesner, C. A., and J. Luhr (2010), Melt inclusion study of the Toba Tuffs, Sumatra, Indonesia, *J. Volcanol. Geotherm. Res.*, *197*, 259–278, doi:10.1016/j.jvolgeores.2010.06.001.

Crutzen, P. J. (2006) Albedo enhancement by stratospheric sulfur injections: A contribution to resolve a policy dilemma? *Clim. Chang.*, *77*(3–4), 211–219, doi:10.1007/s10584-006-9101-y.

Deshler, T. (2008), A review of global stratospheric aerosol: Measurements, importance, life cycle and local stratospheric aerosol, *Atmos. Res.*, *90*, 223–232, doi:10.1016/j.atmosres.2008.03.016.

Dutton, E. G., and J. R. Christy (1992), Solar radiative forcing at selected locations and evidence for global lower tropospheric cooling following the eruptions of El Chichón and Pinatubo, *Geophys. Res. Lett.*, *19*(23), 2313–2316, doi:10.1029/92GL02495.

Echle, G., T. von Clarmann, and H. Oelhaf (1998), Optical and microphysical parameters of the Mt. Pinatubo aerosol as determined from MIPAS-B mid-IR limb emission spectra, *J. Geophys. Res.*, *103*(D15), 19,193–19,211, doi:10.1029/98JD01363.

English, J. M., O. B. Toon, M. J. Mills, and F. Yu (2011), Microphysical simulations of new particle formation in the upper troposphere and lower stratosphere, *Atmos. Chem. Phys.*, *11*, 9303–9322, doi:10.5194/acp-11-9303-2011.

English, J. M., O. B. Toon, and M. J. Mills (2012), Microphysical simulations of stratospheric sulfur geoengineering, *Atmos. Chem. Phys.*, *12*, 4775–4793, doi:10.5194/acp-12-4775-2012.

Fan, T. and O. B. Toon (2011), Modeling sea-salt aerosol in a coupled climate and sectional microphysical model: Mass, optical depth and number concentration, *Atmos. Chem. Phys.*, *11*, 4587–4610, doi:10.5194/acp-11-4587-2011.

Garcia, R. R., D. R. Marsh, D. E. Kinnison, B. A. Boville, and F. Sassi (2007), Simulation of secular trends in the middle atmosphere, 1950–2003, *J. Geophys. Res.*, *112*(D9), D09301, doi:10.1029/2006JD007485.

Garcia, R. R., and W. J. Randel (2008), Acceleration of the Brewer–Dobson circulation due to increases in greenhouse gases. *J. Atmos. Sci.*, *65*(8), 2731–2739. doi:10.1175/2008JAS2712.1.

Giauque, W. F., E. W. Hornung, J. E. Kunzler, and T. R. Rubin (1960), The thermodynamic properties of aqueous sulfuric acid solutions and hydrates from 15-degrees-K to 300-degrees-K, *J. Am. Chem. Soc.*, *82*(1), 62–70.

Graf, H.-F., I. Kirchner, A. Robock, and I. Schult (1993), Pinatubo eruption winter climate effects: Model versus observations, *Clim. Dyn.*, *9*, 81–93.

Guo, S., G. J. S. Bluth, W. I. Rose, I. M. Watson, and A. J. Prata (2004), Re-evaluation of SO2 release of the 15 June 1991 Pinatubo eruption using ultraviolet and infrared satellite sensors, *Geochem. Geophys. Geosyst.*, *5*, Q04001, doi:10.1029/ 2003GC000654.

Hanson, D. R. (2005), Mass accommodation of H_2SO_4 and CH_3SO_3H on water-sulfuric acid solutions from 6% to 97% RH, *J. Phys. Chem. A*, *109* (31), 6919–6927, doi:10.1021/jp0510443.

Heckendorn, P., D. Weisenstein, S. Fueglistaler, B. P. Luo, E. Rozanov, M. Schraner, L. W. Thomason, and T. Peter (2009), The impact of geoengineering aerosols on stratospheric temperature and ozone, *Environ. Res. Lett.*, *4*, 045108, doi:10.1088/1748-9326/4/4/045108.

Jones, G. S., J. M. Gregory, P. A. Stott, S. F. B. Tett, and R. B. Thorpe (2005), An AOGCM simulation of the climate response to a volcanic super-eruption, *Clim. Dyn.*, *25*, 725–738, doi:10.1007/s00382-005-0066-8.

Kinnison, D. E., et al. (2007), Sensitivity of chemical tracers to meteorological parameters in the MOZART-3 chemical transport model, *J. Geophys. Res.*, *112*, D20302, doi:10.1029/2006JD007879.

Kokkola, H., R. Hommel, J. Kazil, U. Niemeier, A.-I. Partanen, J. Feichter, and C. Timmreck (2009), Aerosol microphysics modules in the framework of the ECHAM5 climate model – intercomparison under stratospheric conditions, *Geosci. Model Dev.*, *2*, 97–112, doi:10.5194/gmd-2-97-2009.

Krueger, A. J., L. S. Walter, P. K. Bhartia, C. C. Schnetzler, N. A. Krotkov, I. Sprod, and G. J. S. Bluth (1995), Volcanic sulfur dioxide measurements from the total ozone mapping spectrometer instruments, *J. Geophys. Res.*, *100*, 14,057-14,076.

Kulmala, M., and A. Laaksonen (1990), Binary nucleation of water sulfuric-acid system – Comparison of classical-theories with different H2SO4 saturation vapor-pressures, *J. Chem. Phys.*, *93*(1), 696–701.

Labitzke, K. (1994), Stratospheric temperature changes after the Pinatubo eruption, *J. Atmos. Terrest. Phys.*, *56*(9), 1027–1034, doi:10.1016/0021-9169(94)90039-6.

Labitzke, K., and M. P. McCormick (1992), Stratospheric temperature increases due to Pinatubo aerosols, *Geophys. Res. Lett.*, *19*, 207–210.

Lamarque J.-F., et al. (2010), Historical (1850–2000) gridded anthropogenic and biomass burning emissions of reactive gases and aerosols: methodology and application, *Atmos. Chem. Phys.*, *10*(15), 7017–7039, doi:10.5194/acp-10-7017-2010.

Lin, S. J., and R. B. Rood (1996), Multidimensional flux-form semi-Lagrangian transport schemes, *Mon. Weather Rev.*, *124*(9), 2046–2070.

Lohmann, U., B. Karcher, and C. Timmreck (2003), Impact of the Mount Pinatubo eruption on cirrus clouds formed by homogeneous freezing in the ECHAM4 GCM, *J. Geophys. Res.*, *108*(D18), 4568, doi:10.1029/2002JD003185.

Luo, M., J. M. Russell III, and T. Y. W. Huang (1997), Halogen Occultation Experiment observations of the quasi-biennial oscillation and the effects of Pinatubo aerosols in the tropical stratosphere, *J. Geophys. Res.*, *102*(D15), 19,187–19,198, doi:10.1029/97JD01015.

Mann, G. W., et al. (2012), Intercomparison of modal and sectional aerosol microphysics representations within the same 3-D global chemical transport model, *Atmos. Chem. Phys.*, *12*, 4449–4476, doi:10.5194/acp-12-4449-2012.

Marsh, D. R., Garcia, R. R., Kinnison, D. E., Boville, B. A., Sassi, F., Solomon, S. C., and Matthes, K. (2007). Modeling the whole atmosphere response to solar cycle changes in radiative and geomagnetic forcing. *J. Geophys. Res.*, *112*, 23306. doi:10.1029/2006JD008306.

McCormick, M. P., and R. E. Veiga (1992), SAGE II measurements of early Pinatubo aerosols, *Geophys. Res. Lett.*, *19*, 155–158.

Mergenthaler, J. L., J. B. Kumer, and A. E. Roche (1995), CLAES observations of Mt. Pinatubo stratospheric aerosol, *Geophys. Res. Lett.*, *22*(24), 3497–3500, doi:10.1029/95GL02787.

Mills, M. J., O. B. Toon, R. P. Turco, D. E. Kinnison, and R. R. Garcia (2008), Massive global ozone loss predicted following regional nuclear conflict, *PNAS*, *105*(14), 5307–5312, doi:10.1073/pnas.0710058105.

Minnis, P., E. F. Harrison, L. L. Stowe, G. G. Gibson, F. M. Denn, D. R. Doelling, and W. L. Smith Jr. (1993), Radiative climate forcing by the Mount Pinatubo eruption, *Science*, *259*(5100), 1411–1415.

Neely, R. R., III, J. M. English, O. B. Toon, S. Solomon, M. Mills, and J. P. Thayer (2011), Implications of extinction due to meteoritic smoke in the upper stratosphere, *Geophys. Res. Lett.*, *38*, L24808, doi:10.1029/2011GL049865.

Niemeier, U., C. Timmreck, H.-F. Graf, S. Kinne, S. Rast, and S. Self (2009), Initial fate of fine ash and sulfur from large volcanic eruptions, *Atmos. Chem. Phys.*, *9*, 9043–9057, doi:10.5194/acp-9-9043-2009.

Oman, L., A. Robock, G. L. Stenchikov, T. Thordarson, D. Koch, D. T. Shindell, and C. Gao (2006), Modeling the distribution of the volcanic aerosol cloud from the 1783–1784 Laki eruption, *J. Geophys. Res.*, *111*, D12209, doi:10.1029/2005JD006899.

Oppenheimer, C. (2002), Limited global change due to the largest known Quaternary eruption, Toba 74 kyr BP?, *Quat. Sci. Rev.*, *21*, 1593–1609.

Palmer, K. F., and D. Williams (1975), Optical constants of sulfuric acid: Application to the clouds of Venus? *Appl. Optics*, *14*, 208–219.

Petraglia, M., et al. (2007), Middle Paleolithic assemblages from the Indian subcontinent before and after the Toba Super-Eruption, *Science*, *317*, 114–116, doi:10.1126/science.1141564.

Pinto, J. P., R. P. Turco, and O. B. Toon (1989), Self-limiting physical and chemical effects in volcanic eruption clouds, *J. Geophys. Res.*, *94*(D8), 11,165–11,174.

Pitts, M. C., and L. W. Thomason (1993), The impact of the eruptions of Mount Pinatubo and CERRO Hudson on Antarctic aerosol levels during the 1991 austral spring, *Geophys. Res. Lett.*, *20*(22), 2451–2454, doi:10.1029/93GL02160.

Pueschel, R. F., P. B. Russell, D. A. Allen, G. V. Ferry, K. G. Snetsinger, J. M. Livingston, and S. Verma (1994), Physical and optical properties of the Pinatubo volcanic aerosol: Aircraft observations with impactors and a Sun-tracking photometer, *J. Geophys. Res.*, *99*, 12,915-12,922.

Rampino, M. R., and S. Self (1992), Volcanic winter and accelerated glaciation following the Toba super-eruption, *Nature*, *359*, 50–52.

Read, W. G., L. Froidevaux, and J. W. Waters (1993), Microwave limb sounder measurements of stratospheric SO_2 from the Mt. Pinatubo volcano, *Geophys. Res. Lett.*, *20*, 1299–1302.

Richter, J. H., F. Sassi, R. R. Garcia, K. Matthes, and C. A. Fischer (2008), Dynamics of the middle atmosphere as simulated by the Whole Atmosphere Community Climate Model, version 3 (WACCM3), *J. Geophys. Res.*, *113*, D08101, doi:10.1029/2007JD009269.

Robock, A., C. M. Ammann, L. Oman, D. Shindell, S. Levis, and G. Stenchikov (2009), Did the Toba volcanic eruption of ~74 ka B.P. produce widespread glaciation?, *J. Geophys. Res.*, *114*, D10107, doi:10.1029/2008JD011652.

Rose, W. I., and C. A. Chesner (1987), Dispersal of ash in the great Toba eruption, 75 ka, *Geology*, *15*, 913–917.

Ross, M., M. Mills, and D. Toohey (2010), Potential climate impact of black carbon emitted by rockets, *Geophys. Res. Lett.*, *37*, L24810, doi:10.1029/2010GL044548.

Russell, P. B., et al. (1996), Global to microscale evolution of the Pinatubo volcanic aerosol, derived from diverse measurements and analyses, *J. Geophys. Res.*, *101*, 18,745-18,763.

Sabinina, A. L., and L. Terpugow (1935), Die oberflachenspannung de systems schwefelsaure-wasser, *Z. Phys. Chem. A*, *173*, 237–241.

Sassen, K., D. O.'. C. Starr, G. G. Mace, M. R. Poellot, S. H. Melfi, W. L. Eberhard, J. D. Spinhirne, E. W. Eloranta, D. E. Hagen, and J. Hallett (1995), The 5–6 December 1991 FIRE IFO II jet stream cirrus case study: Possible influences of volcanic aerosols, *J. Atmos. Sci. 52*, 97–123.

Smith, S. J., J. van Aardenne, Z. Klimont, R. Andres, A. Volke, and S. Delgado Arias (2011), Anthropogenic sulfur dioxide emissions: 1850–2005, *Atmos. Chem. Phys.*, *11*, 1101–1116, doi:10.5194/acp-11-1101-2011.

Song, N., D. O.'. C. Starr, D. J. Wuebbles, A. Williams, and S. Larson (1996), Volcanic aerosols and interannual variation of high level clouds, *Geophys. Res. Lett.*, *23*, 2657–2660.

Stenchikov, G., K. Hamilton, A. Robock, V. Ramaswamy, and M. D. Schwarzkopf (2004), Arctic oscillation response to the 1991 Pinatubo eruption in the SKYHI general circulation model with a realistic quasi-biennial oscillation, *J. Geophys. Res.*, *109*, D03112, doi:10.1029/2003JD003699.

Stowe, L. L., R. M. Carey, and P. P. Pellegrino (1992), Monitoring the Mt. Pinatubo aerosol layer with NOAA/11 AVHRR data, *Geophys. Res. Lett.*, *19*, 159–162.

Su, L., and O. B. Toon (2011), Saharan and Asian dust: Similarities and differences determined by CALIPSO, AERONET, and a coupled climate-aerosol microphysical model, *Atmos. Chem. Phys.*, *11*, 3263–3280, doi:10.5194/acp-11-3263-2011.

Tabazadeh, A., O. B. Toon, S. L. Clegg, and P. Hamill (1997), A new parameterization of H_2SO_4/H_2O aerosol composition: Atmospheric implications, *Geophys. Res. Lett.*, *24*, no. 15, 1931–1934.

Thomas, M. A., C. Timmreck, M. A. Giorgetta, H.-F. Graf, and G. Stenchikov (2009), Simulation of the climate impact of Mt. Pinatubo eruption using ECHAM5 – Part 1: Sensitivity to the modes of atmospheric circulation and boundary conditions, *Atmos. Chem. Phys.*, *9*, 757–769, doi:10.5194/acp-9-757-2009.

Timmreck, C., H.-F. Graf, and I. Kirchner (1999), A one and half year interactive MA/ECHAM4 simulation of Mount Pinatubo Aerosol, *J. Geophys. Res.*, *104*(D8), 9337–9359, doi:10.1029/1999JD900088.

Timmreck, C., and Graf, H.-F. (2006), The initial dispersal and radiative forcing of a Northern Hemisphere mid-latitude super volcano: A model study, *Atmos. Chem. Phys.*, *6*, 35–49, doi:10.5194/acp-6-35-2006.

Timmreck, C., H.-F. Graf, S. J. Lorenz, U. Niemeier, D. Zanchettin, D. Matei, J. H. Jungclaus, and T. J. Crowley (2010), Aerosol size confines climate response to volcanic super-eruptions, *Geophys. Res. Lett.*, *37*, L24705, doi:10.1029/2010GL045464.

Toohey, M., K. Krüger, U. Niemeier, and C. Timmreck (2011), The influence of eruption season on the global aerosol evolution and radiative impact of tropical volcanic eruptions. *Atmos. Chem. Phys. 11*, 12351–12367, doi:10.5194/acp-11-12351-2011.

Toon, O. B., R. P. Turco, D. Westphal, R. Malone, and M. S. Liu (1988), A multidimensional model for aerosols - Description of computational analogs, *J. Atmos. Sci.*, *45*, 2123–2143.

Trepte, C. R., and M. H. Hitchman (1992), Tropical stratospheric circulation deduced from satellite aerosol data, *Nature*, *355*, 626–628.

Vernier, J.-P., et al. (2011), Major influence of tropical volcanic eruptions on the stratospheric aerosol layer during the last decade, *Geophys. Res. Lett.*, *38*, L12807, doi:10.1029/2011GL047563.

Wang, P. H., P. Minnis, and G. K. Yue (1995), Extinction coefficient (1 μm) properties of high-altitude clouds from solar occultation measurements (1985–1990): Evidence of volcanic aerosol effect, *J. Geophys. Res.*, *100*, No. D2, 3181–3199.

Weisenstein, D. K., J. E. Penner, M. Herzog, and X. Liu (2007), Global 2-D intercomparison of sectional and modal aerosol modules, *Atmos. Chem. Phys.*, *7*, 2339–2355, doi:10.5194/acp-7-2339-2007.

WMO (1957), Meteorology-A three-dimensional science, *WMO Bull.*, *6*, 134–138.

Young, R. E., H. Houben, and O. B. Toon (1994), Radiatively forced dispersion of the Mt. Pinatubo volcanic cloud and induced temperature perturbations in the stratosphere during the first few months following the eruption, *Geophys. Res. Lett.*, *21*, 369–372.

Zhao, J., and R. P. Turco (1995), Nucleation simulations in the wake of a jet aircraft in stratospheric flight, *J. Aerosol Sci. 26*(5), 779–795.